Proceedings of the ASME 2016 Manufacturing Science and Engineering Conference
ASME MSEC 2016
June 27-July 1, 2016, Blacksburg, Virginia, USA

MSEC2016-8692

IDENTIFYING UNCERTAINTY IN LASER POWDER BED FUSION MODELS

Felipe Lopez
Department of Mechanical Engineering
University of Texas at Austin
Austin, TX 78712
Email: felipelopez@utexas.edu

Paul Witherell, Brandon Lane
Engineering Laboratory
National Institute of Standards and Technology
Gaithersburg, MD 20899
Email: [paul.witherell, brandon.lane]@nist.gov

ABSTRACT

A limitation frequently encountered in additive manufacturing (AM) models is a lack of indication about their precision and accuracy. Often overlooked, information on model uncertainty is required for validation of AM models, qualification of AM-produced parts, and uncertainty management. This paper presents a discussion on the origin and propagation of uncertainty in Laser Powder Bed Fusion (L-PBF) models. Four sources of uncertainty are identified: modeling assumptions, unknown simulation parameters, numerical approximations, and measurement error in calibration data. Techniques to quantify uncertainty in each source are presented briefly, along with estimation algorithms to diminish prediction uncertainty with the incorporation of online measurements. The methods are illustrated with a case study based on a transient, stochastic thermal model designed for melt pool width predictions. Model uncertainty is quantified for single track experiments and the effect of online estimation in overhanging structures is studied via simulation. The application of these concepts to estimation and control of the L-PBF process is suggested.

Keywords: additive manufacturing, uncertainty quantification, melt pool width.

INTRODUCTION

Some have referred to additive manufacturing (AM) as the third industrial revolution [1]. AM is the use of layer-based processes for producing parts directly from computer (CAD) models, without part-specific tooling [2]. Since its introduction in the mid-1980s [3, 4], AM has become popular because of its ability to produce parts that were impossible with traditional manufacturing techniques. After decades of being limited to polymer prototypes, these technologies are now employed in the production of functional parts made of polymers, ceramics, and metals [5–7].

AM technologies still present some unresolved challenges that hinder their widespread adoption. Among these challenges are process variability, unsatisfactory part quality, and lack of process standards; all of which originate from the limited knowledge of this relatively new set of processes. Numerous models have been developed to improve the understanding of these processes and to predict the quality of AM-produced components. Although most models published in the literature have been compared with experimental measurements, they often lack measures of the precision and accuracy of their predictions.

Knowledge of uncertainty in AM models is required for applications such as:

(a) Model validation, which may use comparisons between simulation results and experimental data, accounting for uncertainty in both sources. Comparison of simulation results obtained with different models is expected to require information on their uncertainty as well.
(b) Decision making, where model predictions and their prob-

abilities may be used to make informed decisions. In the case of AM, for example, one would expect to use models to certify AM-produced parts. Model-enabled certification will depend on the probability of predicted key performance indicators being within admissible bounds.

(c) Uncertainty management, to identify the sources with the largest relative contributions to overall prediction error, and determine effective strategies to more accurate predictions.

This paper presents a general discussion on uncertainty in computational models of metal-based AM, and in particular, of Laser Powder Bed Fusion (L-PBF). The discussion begins with how key performance indicators (KPIs) drive the development of models, seeking simulation as a method to be used for qualification of L-PBF produced parts. We present a general description of the modeling process, and the generation and propagation of errors. We then conduct a deep dive into how errors are commonly introduced into AM models, and the contribution of each individual error source in such predictions. Uncertainty quantification (UQ) methods suitable for the L-PBF process are discussed, and Bayesian estimation is presented as a method to extend UQ by including online measurements to reduce overall prediction uncertainty. These concepts are illustrated on a low-order stochastic model.

The contribution in this paper is three-fold. It provides: 1) A discussion on methods for uncertainty quantification in L-PBF models; 2) An example of uncertainty quantification for computational models in which all sources of error are considered; and 3) A method for quantifying unmodeled process perturbations with potential applications in detection of anomalies and feedback control.

BACKGROUND

In the AM community, computational models are sought after as means to predict the outcome of physical processes. The choice of KPIs to be predicted depends on the application that is intended for the model. A common aim among modelers is model-based qualification, which will require control of several qualities: identification and reduction of defects, dimensional accuracy and surface finish, microstructure and mechanical properties, and reduction of residual stresses. In this article, it is suggested that melt pool dimensions be chosen as KPIs due to their direct relationship with the thermal processes that define these qualities[1]. Among the set of melt pool dimensions, width is chosen as the primary KPI in this first study because it can be traced both during and after the build.

Several other heat transfer models have been published in the literature with similar goals [12–19]. Though different in their formulation, as AM models, and even more specific, as L-PBF models, it is expected that at the highest levels of abstraction, sources of information and sources of error share common characteristics. A study of common uncertainty sources in L-PBF models has not been reported yet.

Until recently, the issues of model validation and verification (V&V) and uncertainty quantification (UQ) had for the most part eluded the AM community. Some of the few examples of UQ in AM models can be found in the papers by Moser [20] and Ma [21], both of which studied the sensitivity of their models to uncertainty in input parameters; and King [22], who discussed uncertainty quantification methods for surrogate models.

In engineering, computational models are designed as approximations of physical reality and, as such, are subjected to a cascade of errors and uncertainties. Figure 1 illustrates recognized sources of modeling errors [23], that we have adapted for an additive manufacturing application. Introduction of errors begin as early as the selection of the physical process to model (e.g. heat diffusion, melting/solidification, free-surface flows, etc.), which is approximated with an imperfect model of reality given by constitutive equations. All physical information that cannot be represented by the adopted mathematical model is considered to be modeling error. The mathematical model is calibrated with incomplete information of model parameters, based on incomplete calibration data gathered with imperfect sensors. Error in the determination of simulation parameters is propagated through the simulation. The mathematical model, often unsolvable with analytical methods, is approximated with a numerical method to result in a solvable form for simulation. Such approximations inject numerical errors that undermine the accuracy of the numerical predictions of the quantity of interest. Additionally, in the case of model validation, measurement error must be kept in mind for comparisons between simulation results and test data.

[1]Common L-PBF defects can be classified in two broad types: under-melting and over-melting defects. The former are generated by incomplete melting or improper fusion between successive tracks or layers [8], while the latter are caused by entrapment of gases or improper closure of a keyhole [9]. Both types have a strong influence on tensile, fatigue and hardness properties. Dimensional accuracy of the produced part is dependent on the degree of under- and over-melting too, especially in external tracks. Both for defect prevention and dimensional accuracy, the shape of the melt pool has traditionally been used as an indicator of under- and over-melting.

Grain size and morphology (key microstructural parameters that define yield strength and other mechanical properties) are dependent on the thermal history during solidification. In the case of Ti-6Al-4V, for example, grain size is known to be dependent on cooling rates, which are in turn functions of the cross-sectional area of the melt pool. Grain morphology, on the other hand, depends on the melt pool length-to-depth ratio [10].

Residual stresses, known to have a strong bearing on the fatigue crack growth, are linked to thermal cycles in the part. Large thermal gradients near the laser spot, rapid cooling, and repetition of this process produce localized compression and tension [11]. Some techniques used to mitigate residual stresses are the choice of appropriate scanning patterns, *in situ* heating, and *ex situ* heat treatment.

Even in the case of an optimal scanning pattern, the quality of an L-PBF-produced part can still be improved with accurate and responsive thermal control of melt pool dimensions.

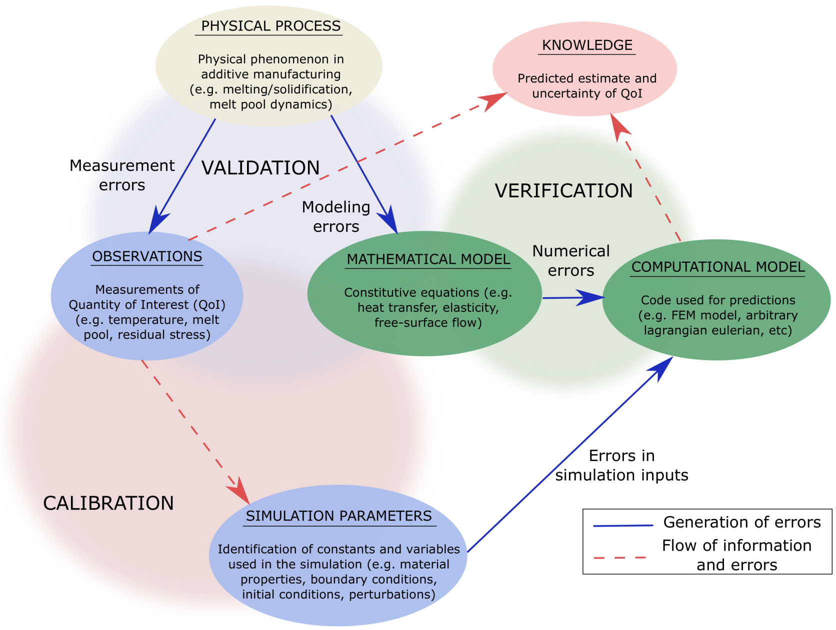

FIGURE 1: Cascade of sources of error in computer models of additive manufacturing.

IDENTIFYING UNCERTAINTY IN L-PBF MODELS

All the aforementioned sources of error are present in L-PBF process models. L-PBF involves multiple physical phenomena occurring at different length scales. The process is controlled by thermal, free-surface flow, structural and microstructural processes, which are closely coupled. Due to the complexity of the process, most computational models limit their scope to a subset of physical phenomena at a given scale, neglecting dynamics not captured by them. Modeling assumptions that neglect certain dynamics are the origin of modeling uncertainty[2]. It should be noted that only relationships of the causal type contribute to modeling uncertainty. For instance, if temperature distribution or a similar variable is chosen as the KPI, the lack of a structural model would not result in a relevant contribution to modeling uncertainty because the systems are only weakly coupled and the effect of stresses on the thermal history is insignificant.

Some common examples of modeling uncertainty in L-PBF can be found in surface tension and particle-level dynamics neglected in continuum models[3], the choice of inaccurate distributions for laser power acting on the powder bed, or an inappropriate choice of boundary conditions that neglects track-to-track and layer-to-layer interactions[4].

Input uncertainty is the result of inaccurate simulation parameters, adopted in lieu of more precise knowledge or as result of uncertainty in the training data. In the case of L-PBF models, common sources can be found in: a) absorption coefficient, which quantifies the amount of irradiated laser power that heats up the powder bed; b) thermal conductivity in loose powder, which depends on the distribution of powder particles; c) thermo-physical parameters at high temperatures; d) convection and radiation coefficients; and e) enhancing coefficients occasionally used to account for the effect of advection in the liquid phase. It is difficult to determine the precise values of these parameters for use in L-PBF models, and it is common to observe them used only as adjusting coefficients.

Various numerical methods have been used to solve the chosen mathematical models. Even when commercial packages based on finite element methods are common in academia and industry, other methods (e.g. discrete element methods, arbitrary Lagrangian Eulerian, lattice Boltzmann methods) are rapidly capturing the attention of the AM community. The choice of the numerical method depends on the physical processes included in the mathematical model (some methods are tailored for free-surface and particle-to-particle interactions), and their suitability for parallelization and implementation in high performance computing (HPC) systems. In any case, a choice of numerical method will result in an approximation error that depends on the granularity of the chosen grid. Commercial packages used for L-PBF models include convergence studies to ensure that the error

[2] The approach followed in this article makes no distinction between aleatory variability and epistemic uncertainty, and accounts only for their joint effect, as suggested in [24].

[3] Particles in the powder bed, randomly packed and a source of aleatory variability, heat up and melt creating stochastic variations in melt pool morphology.

[4] During the build, variations in thermal diffusivity in material surrounding the melt pool can have differences of up to two orders of magnitude between fully-dense material and loose powder. This effect has been observed experimentally when melting overhanging structures, where larger (almost three times) than usual melt pool areas have been observed [25].

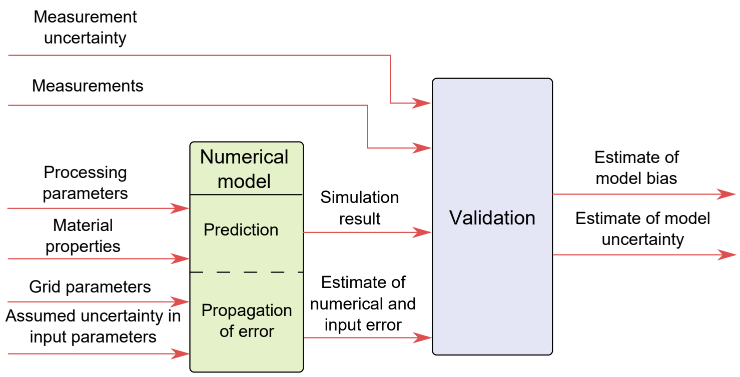

FIGURE 2: V&V and UQ in computational models as suggested in ASME V&V 20.

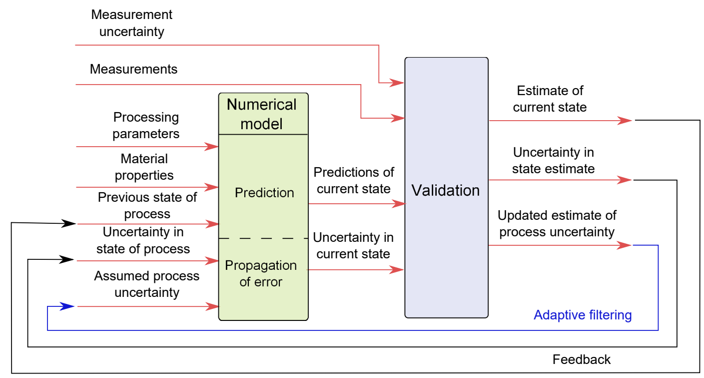

FIGURE 3: Online estimation in predictive models.

is small, but its magnitude is seldom reported.

Measurement uncertainty is independent of the choice of numerical model, and depends solely on the methods and instruments used to gather test data. The choice of appropriate measurement techniques for L-PBF is an unsolved issue, and it depends on the KPI of interest [26]. In the case of thermal variables, non-intrusive thermographic techniques hold the promise of providing online temperature measurements in the powder bed, but difficulties determining the correct emissivity of the material makes these predictions partially unreliable.

It is apparent that the different sources of uncertainty can only be conceptualized but not completely defined until the mathematical model and measurement system are selected. This discussion will be expanded in the section dedicated to our case study, where each source will be identified and quantified.

UNCERTAINTY QUANTIFICATION

Quantification of uncertainty in computational models is based on the comparison of simulation solutions with experimental data, to identify and track every source of error [23]. A comprehensive discussion on uncertainty sources in heat transfer and fluid mechanics models can be found in the standard ASME V&V 20, along with methods to quantify them [27]. The fact that AM involves thermally-activated consolidation processes makes this standard suitable for this application. Figure 2 illustrates the process of prediction and validation followed in UQ with ASME V&V 20.

In this example, a known set of processing parameters and material properties are fed to the model to obtain a simulation result S. Information about the grid is used to estimate the numerical error δ_{num} that results from the numerical method using methods based on Richardson's extrapolation or Roache's grid convergence index (GCI). Meanwhile, an assumed probability distribution in simulation parameters is propagated through the model into the predicted quantity of interest, resulting in an estimate of the error due to inaccurate inputs δ_{input}. Finally, simulation results S are confronted with measurements D and measurement error δ_D. The difference between model prediction and measurement determines the bias E, which acts as an estimate of modeling error δ_{model}. All sources of error are merged in the calculation of prediction uncertainty, which is reported along the bias as described in the first section of ASME V&V 20.

It is a well-known fact that the L-PBF process is highly variable. Heat transfer fluctuates throughout the entire build as a result of variations in processing conditions (laser power, scan speed, layer thickness, etc.), thermal diffusivity surrounding the melt pool, and random packing in the powder bed. Failure to include these sources of variability will result in unreliable melt pool width predictions.

Process variability is accounted for as uncertainty due to unknown inputs, if it can be traced back to simulation parameters, or as modeling uncertainty otherwise. Herein, we describe an application of Bayesian estimation to reduce modeling error by mapping sources of variability to random simulation parameters that are identified in real time and used in the calculation of more meaningful predictions. In the case of L-PBF, the set of identified parameters may include random variables that attempt to model the variable thermal characteristics of the material that surrounds the melt pool. Following this strategy, measurements can be used to detect these perturbations and sequentially readjust simulation parameters.

The process for online estimation is illustrated in Figure 3. In this case, a simulation is performed for a given set of simulation parameters and an initial state with its associated uncertainty, which originate from a previous step of the simulation (feedback). Uncertainty in the initial state is propagated in time using the model and process uncertainty, which is expected to capture the effect of modeling error, numerical error δ_{num} and error due to unknown inputs δ_{input}. The propagated state and uncertainty are then compared with the measurement and its error δ_D to result in estimates of the state at the next time step, its uncertainty, and an updated estimate of process uncertainty in the case of adaptive filtering.

$$\frac{dy_1}{dt} = -\frac{2\mu\alpha_1}{y_1}\left(\frac{y_2}{y_2-y_1}\right) - \frac{A\times P}{\pi\rho C_p \Delta T y_1^2}\left(1+\frac{v}{2\mu\alpha_1}y_1\right)\exp\left(-\frac{v}{2\mu\alpha_1}y_1\right) + \frac{v^2}{4\mu\alpha_1}\frac{T_1-A_l}{\Delta T}(y_2-y_1) \tag{1}$$

$$\frac{dy_i}{dt} = -\frac{\mu\alpha_i}{y_i}\left(\frac{y_{i+1}}{y_{i+1}-y_i} - \frac{y_{i-1}}{y_i-y_{i-1}}\right) + \frac{v^2}{8\mu\alpha_i}\frac{T_i-A_l}{\Delta T}(y_{i+1}-y_{i-1}), \quad \text{for } i=2,3,\ldots,m-1 \tag{2}$$

$$\frac{dy_m}{dt} = -\frac{\mu\alpha_m}{(1+Ste^{-1})y_m}\left(\frac{y_{m+1}}{y_{m+1}-y_m} - \frac{y_{m-1}}{y_m-y_{m-1}}\right) - \frac{v^2}{4\mu\alpha_m(1+Ste^{-1})}\frac{A_l-2T_m+T_0}{\Delta T}\left(\frac{1}{y_{m+1}-y_m} + \frac{1}{y_m-y_{m-1}}\right)^{-1}\left\{1+2Ste^{-1}\left[1+\left(\frac{A_l-2T_m+T_0}{\Delta T}\frac{v}{2\mu\alpha_m}\right)^2\left(\frac{1}{y_{m+1}-y_m}+\frac{1}{y_m-y_{m-1}}\right)^{-2}\right]^{-1}\right\} \tag{3}$$

$$\frac{dy_i}{dt} = -\frac{\mu\alpha_i}{y_i}\left(\frac{y_{i+1}}{y_{i+1}-y_i} - \frac{y_{i-1}}{y_i-y_{i-1}}\right) + \frac{v^2}{8\mu\alpha_i}\frac{T_i-T_0}{\Delta T}(y_{i+1}-y_{i-1}), \quad \text{for } i=m+1,\ldots,N-1 \tag{4}$$

$$\frac{dy_N}{dt} = -\frac{\mu\alpha_N}{y_N}\left(\frac{y_N-2y_{N-1}}{y_N-y_{N-1}}\right) - \frac{v^2}{4\mu\alpha_N}(y_N-y_{N-1}). \tag{5}$$

It can be seen that both approaches have the same sources of uncertainty, the only difference being that some sources of process variability that are included either as modeling error or error due to unknown inputs in offline models are mapped to a random initial state.

CASE STUDY: UNCERTAINTY IN A STOCHASTIC MODEL FOR L-PBF

In this case study, an Isotherm Migration Method (IMM) model, developed for laser cladding [28], is adjusted for use in L-PBF. The model provides a set of ordinary differential equations (ODEs) that describe the motion of isotherms on the surface of the powder bed. If one of these isotherms is assigned to the melting temperature (T_m), the model can be used to dynamically track the location of the solidification front and predict melt pool width. The method is similar to Rosenthal's solution for temperature distribution due to a moving point source [29], but it allows the use of temperature-dependent material properties. Also, instead of solving for the distribution of temperature $T(x,y,z,t)$, the system is solved for the half-widths $y(T,t)$ of isotherms on the bed surface[5]. The array of half-widths corresponds to a user-defined, uniformly-spaced temperature grid $T = [T_1 \quad T_2 \quad \ldots \quad T_m \quad \ldots \quad T_N]$, for $\Delta T < 0$.

The computational model shown in equations (1) to (5) describes the evolution of the half-widths $y = [y_1 \quad y_2 \quad \ldots \quad y_m \quad \ldots \quad y_N]$, where each half-width y_i corresponds to a temperature T_i[6]. The set of ODEs can be expressed in compact form as $\dot{x} = f(x,u)$, where $x = [y \quad \mu]$ denotes the vector of state variables and $u = [P \quad v]$ the vector of control inputs. In this case, μ is the diffusion efficiency, a random variable used to correct for variable sideways thermal diffusion due to unmodeled process perturbations (modeling error is mapped to a simulation variable). Its value is set to 1 in nominal cases, when the melt pool is surrounded by fully-dense material. In the case of of overhanging structures, for example, a decrease of thermal diffusivity toward the bottom improves heat transfer to the sides, increasing the value of μ.

The system of equations is stable for positive thermal diffusivity α, and can be simulated until convergence to a steady-state melt pool width $w_{max} = w_{max}(P,v,A,h_l,T_m,\alpha(T))$. The same model can be assembled in the form of an equation that maps the present state vector $x_n = x(t_n)$ to a future instant $t_{n+1} = t_n + \Delta t$, using a forward Euler scheme of the form $x_{n+1} = x_n + f(x_n,u_n) \times \Delta t$, for example.

Uncertainty quantification

Uncertainty is quantified by comparing simulation results for fully-dense material with melt pool width measurements gathered using an EOSINT M270 system on an IN625 plate, as described by Montgomery [30]. Single bead tests were performed using different combinations of laser power and scan speed, both on a bare plate (no added powder) and one with a 20

---

[5]The width of an isotherm under the heat source is twice y, because y is measured from the heat source location to the isotherm. Maximum melt pool width is calculated assuming an ellipse for the isotherms [28].

[6]In these equations, α_i denotes the thermal diffusivity evaluated at temperature T_i, A is the absorption coefficient, P is laser power, ρ is density, C_p is specific heat, v is scan speed, $A_l = T_0 - h_l/(C_p + 2\mu\alpha_i C_p/v/y_m + 2\mu^2\alpha_i^2 C_p/y_m^2/v^2)$ is the apparent ambient temperature for the liquid phase, and $Ste = -C_p\Delta T/h_l$ is the Stefan number.

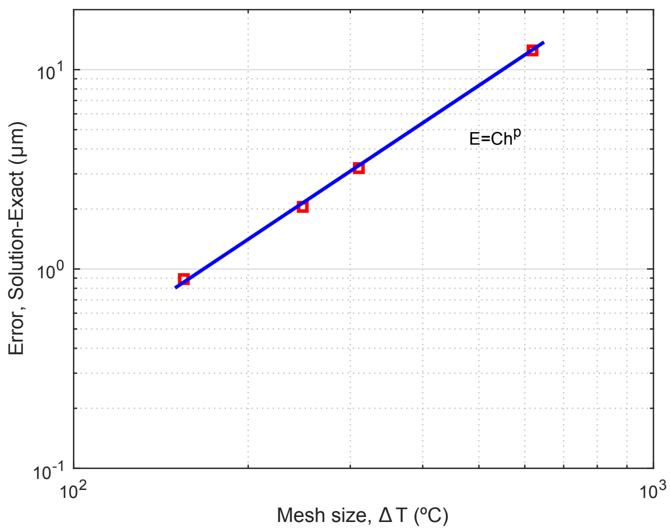

FIGURE 4: Numerical error as a function of mesh size.

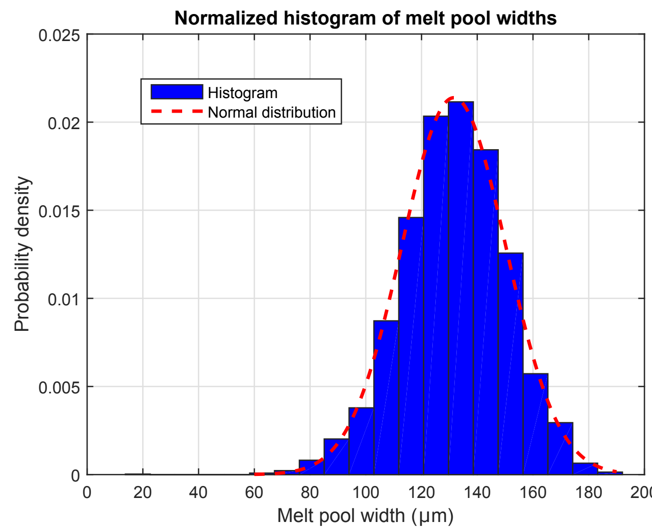

FIGURE 5: Normalized histogram of predicted melt pool widths.

μm layer of powder added. To ensure that diffusion efficiency does not introduce extra uncertainty, only scans on bare plate are compared with model predictions.

Error is approximated within the interval $\delta_{model} \in [E - u_{val}, E + u_{val}]$ centered around $E = S - D$, the bias between the simulation result S and experimental measurements D. Validation uncertainty u_{val}, which accounts for uncertainty from all sources, can be computed following $u_{val} = \sqrt{u_{num}^2 + u_{input}^2 + u_D^2}$ under the assumption that all error sources are independent.

The first steps toward quantification of modeling error are code and solution verification; in other words, assessing that the code is correct (free of bugs) and estimating the error in the numerical approximation. Code was verified with a manufactured solution and it was observed that the method converges to the analytical solution given by Rosenthal for constant material properties as $\Delta T \rightarrow 0$ and $T_{max} \rightarrow \infty$. Similar convergence studies were performed for predictions of melt pool width w (in μm) using temperature-dependent material properties. Results are presented in Figure 4, where successive grid refinement was used to identify an order of accuracy of $p = 1.9$[7].

Numerical uncertainty was quantified using Roache's Grid Convergence Index (GCI) [27] for the prediction obtained with $T_1 = 2560\ ^\circ C$ and $\Delta T = -248\ ^\circ C$, corresponding to a grid of 10 isotherms[8]. The GCI is an estimated 95 % uncertainty (a common uncertainty target) obtained by multiplying the absolute value of a Richardson extrapolation error by an empirically determined factor of safety. In this case, the numerical prediction for melt pool width for L-PBF of Inconel 625 with 195 W and 800 mm/s is $(127.3 \pm 2.7)\ \mu m$ (± 2.12 %).

The second source of uncertainty comes from imperfect knowledge of input parameters, and the effect they may have on predictions. Six factors were selected for a Monte Carlo study to determine the propagation of uncertainty in inputs: laser power (P), scan speed (v), absorption coefficient (A), latent heat (h_l), melting temperature (T_m), and thermal diffusivity ($\alpha_i(T_i)$)[9]. Normal distributions are assumed for the input parameters following:

Input	Nominal	Std. dev. (% nominal)
P	195 W	2.5%
v	0.800 m/s	1.5%
A	0.6	25%
h_l	2.97×10^5 J/kg	5.0%
T_m	1320 °C	5.0%
α_i	$\alpha_i(T_i)$	10.0%

A Monte Carlo approximation of the probability distribution of melt pool width is obtained following $p(w) \propto \sum_{n=1}^{N} \delta_{w_{max}(P^n, v^n, A^n, h_l^n, T_m^n, \alpha^n(T))}$, where δ denotes the Dirac delta and the superscript n indicates the n-th sample of the input parameters. The resulting distribution of predicted melt pool widths (for 4000 samples) resembles a normal distribution, as illustrated in Figure 5, where the 95 % confidence interval is found in $(131.6 \pm 37.3)\ \mu m$.

The last source of uncertainty comes from the experiments used for validation. This study uses measurements that were taken in the middle of the long edge of the single bead track,

[7] The formal order of accuracy of the method was found at $p = 3$, but nonlinearities in the temperature-dependent properties insert iteration error reducing the effective value of p.

[8] The reason to choose a relatively coarse grid is the desire to accelerate the computation by keeping the dimensionality of the IMM model low. This is going to be more important in the case of online predictions, to be described in the next section.

[9] Temperature dependent material properties were obtained with the TCN16 thermodynamic database within the Thermo-Calc software [31].

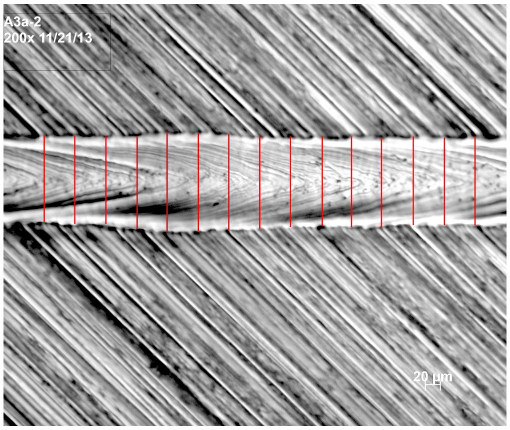

FIGURE 6: Sample image with measurement points marked (No powder added, 125 W and 600 mm/s) [30].

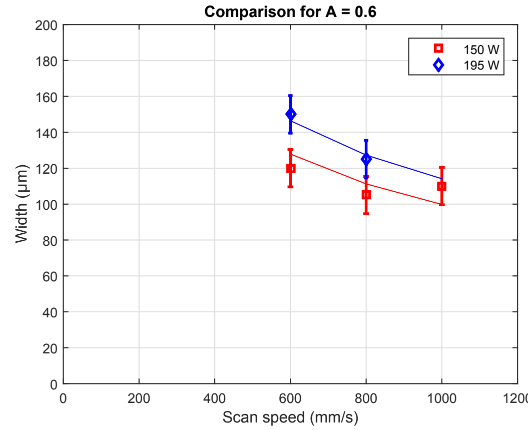

FIGURE 7: Comparison of model predictions with experiments.

which was imaged using a Zeiss AxioVision AX10 optical microscope. The image was then measured 15 times along the width at approximately equal spacing, as shown in Figure 6. These 15 measurements were then averaged for each melt pool. In this study, measurements in the steady-state region have standard deviations of close to 5.2 μm, suggesting a ± 10.4 μm confidence interval.

Measured melt pool widths are shown in Figure 7 and compared to predictions obtained from the IMM model, only for data points close to nominal operating conditions (195 W and 800 mm/s). The region of calibration for this model was delimited between 150 W and 195 W, and 600 mm/s and 1000 mm/s[10]. Assuming that all error sources are independent, validation uncertainty is estimated at (127.3 ± 38.8) μm (± 30.5 %) for nominal conditions. Some observations can be made from these results:

(a) Modeling uncertainty is relatively large, as expected due to the simplification of the thermal problem by assuming a point source instead of a distributed one. The absence of other physical phenomena considered important for melt pool dynamics, such as surface tension, only increases modeling error.
(b) Numerical uncertainty is negligible compared to uncertainty due to unknown input parameters or to experimental error, even for highly-coarse grids.
(c) Error due to uncertainty in input parameters, the error source most widely studied, has a very significant contribution to model uncertainty (± 29.3 %). This is partly due to the large uncertainty assumed for the absorption coefficient A, which was used as a tuning coefficient in this example.
(d) Uncertainty due to unknown inputs depends on the confidence in the chosen set of input parameters. Different users may choose different input uncertainties, resulting in different prediction uncertainties.
(e) It is currently not possible to assess how this model compares to the predictions obtained with other L-PBF models as their uncertainty has not been reported.
(f) The relatively large prediction uncertainty (± 30.5 %) is compensated by the speed of the model. The model returns a melt pool width prediction in 0.1 s when implemented in MATLAB R2014b running on an Intel Core i7-3770 CPU.
(g) Extrapolation of the modeling error to the other points in the region of calibration matches the obtained measurements, as observed in Figure 8, where power and scan speed were kept constant. It is important not to extrapolate predictions outside the region of calibration of each predictive model, which is often not reported.
(h) Model was validated by comparison with scans on bulk material, ignoring the addition of a powder layer. Montgomery reported that the effect of adding a layer of powder does not have a significant effect on melt pool width [30], but its effect was not quantified in this study.

Bayesian estimation

Diffusion efficiency may be allowed to vary in time to account for unmodeled track-to-track and layer-to-layer interactions, which were ignored in the previous example. In this section, we present an example that illustrates how online thermographic monitoring can be used to identify unmodeled dynamics (modeling error) and decrease uncertainty in melt pool width predictions.

The presented case, illustrated in Figure 9, is designed to represent a horizontal overhanging plane which is scanned in a direction perpendicular to the solid-to-powder transitions. This case study, designed and published by Kruth *et al.* [25], showed that melt pool area increases threefold when going through this kind of overhangs. Synthetic data was generated to mimic this

[10]The choice of the region of calibration was arbitrary, and it was chosen as an area around the nominal point where the same absorptivity is able to replicate observed melt pool widths.

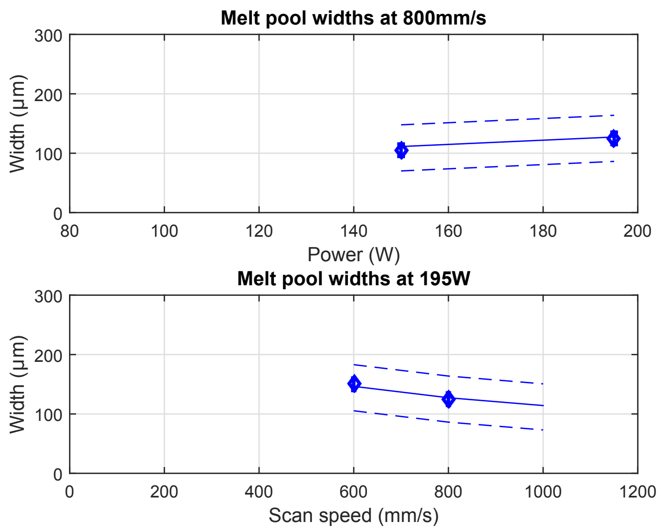

FIGURE 8: Melt pool width predictions for DMLS of Inconel 625.

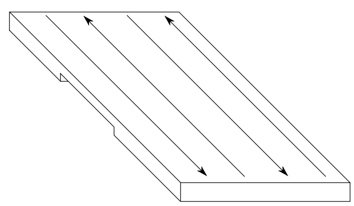

FIGURE 9: Case simulated in "perturbed" scenario.

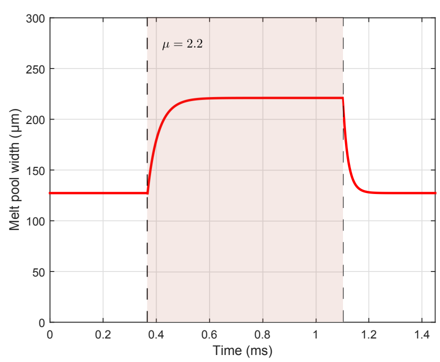

FIGURE 10: Simulation of melt pool width through overhang assuming $\mu = 2.2$.

event by artificially perturbing μ and assuming that it varies instantaneously from 1 to 2.2[11] when melting on top of loose powder.

In this study, it has been assumed that the isotherms corresponding to $T_i = \{576, 824, 1072\}^\circ C$ can be detected with ther-

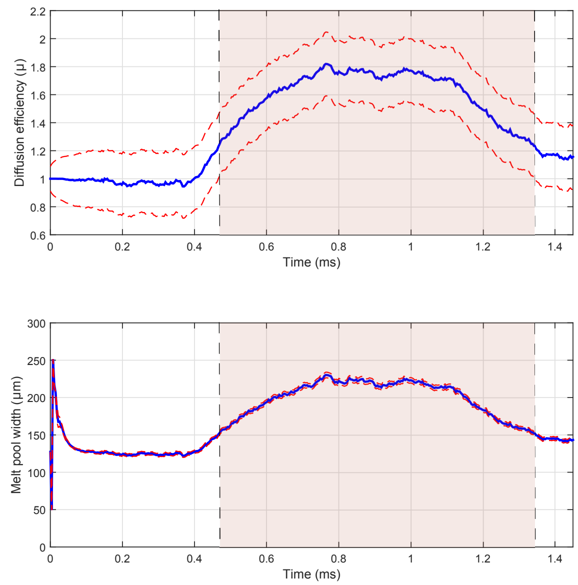

FIGURE 11: Estimated diffusion efficiency and melt pool width. Predictions are shown in blue and 95 % confidence intervals are in dashed red lines.

mographic sensors. To simulate measurement uncertainty, noise was added to the measured isotherm widths following a standard deviation of 26 μm[12].

Process estimation, using a linear stochastic version of the IMM model and a Kalman filter [32], results in the estimates shown in Figure 11, where the null hypothesis of normal operation (no overhang, $H_0 : \mu = 1$) is rejected in favor of the alternative hypothesis of an anomaly ($H_A : \mu \neq 1$) in the shaded region. The perturbation in heat diffusion is detected between 0.47 ms and 1.35 ms, lagging from the 0.37 ms and 1.10 ms in which they occur in the simulation.

Response speed, and accuracy and uncertainty in the estimates are expected to be dependent on the process and measurement uncertainty used for estimation, which were assumed in this example and will have to be adjusted in an experimental study to close the loop shown in Figure 3.

An important point to be observed is the low uncertainty in the melt pool width prediction even in the region of anomalous operation. Without online measurements, models would have to account for the potential variation in diffusion efficiency using large uncertainties for μ, increasing uncertainty in melt pool width predictions. For example, if the study to determine sensitivity to input parameters is repeated letting μ vary following $\mu \sim \text{Unif}[1.0, 2.5]$, the obtained prediction is (193.6 ± 106.6) μm (± 55.1 %), which is much larger than the confidence intervals reported in Figure 11 (± 4.0 μm).

[11] The value of the assumed perturbed diffusion efficiency was chosen to increase steady-state melt pool width approximately by $\sqrt{3}$, assuming that melt pool length changes by the same ratio and the overall melt pool area increases threefold.

[12] The assumed measurement noise used for the synthetic data corresponds to a standard deviation of half the pixel width in similar thermographic settings.

FUTURE WORK

The identification and quantification of the uncertainty sources in the proposed stochastic AM model is not complete until the process uncertainty assumed for diffusion efficiency is validated. Validation of model variability will only be possible in a sequential manner, by comparing model predictions with measurements. Melt pool width measurements need to be taken faster than the characteristic response time of the process, which the model identified in the order of hundredths of milliseconds for L-PBF of Inconel 625 with nominal conditions. At such high data acquisition rates, both gathering and processing the data will be challenging.

This study is scheduled to be performed in the powder bed fusion test bed that NIST is developing for studies of advanced metrology, estimation and control [33]. Once the test bed and the data acquisition system for melt pool widths are ready, the stochastic model presented in this article can be used in the design of an online monitoring system. NIST is currently working on the development of such a system to:

(a) Detect and quantify thermal perturbations and their uncertainties in the L-PBF process, which will allow engineers to locate the regions of the produced part that are most likely to have manufacturing defects.
(b) Design of a feedback process controller, which will use information of the current state of the process.

CONCLUSIONS

As metal-based AM gains popularity, closer attention has been paid to the computational models developed to predict quality in manufactured components. One aspect that has been traditionally ignored in these models is that, if they are to be used in model validation or for certification of parts, one must know how accurate and precise these models are. Uncertainty quantification presents a set of challenges that have often been ignored both by manufacturing and modeling engineers.

The series of steps that go from a physical process to a numerical representation involve successive assumptions in the mathematical models, model parameters, numerical scheme, and calibration data. It is important to quantify the relative effect of each error source to identify the ones that will result in the most significant reductions in prediction uncertainty.

A method to decrease modeling error, by mapping it to random simulation inputs that are identified in real time, is illustrated. Inclusion of random inputs requires that the assumed randomness is validated (and adjusted, if necessary). Adaptive filtering techniques are being evaluated for implementation in a future online monitoring study.

Even though the case study presented in this paper is based on a low-order model, the same ideas can be extended to high-order models. The algorithms used for uncertainty quantification, however, are different. For instance, the high computational cost of Monte Carlo methods prevents their application in the propagation of uncertainty in input parameters. Methods based on the Karhunen-Loève expansion (e.g. polynomial chaos [34]) are often preferred in such scenarios.

ACKNOWLEDGMENT

The authors gratefully acknowledge the comments and suggestions provided by Wim Devesse, developer of the laser cladding model adapted for this study; Colt Montgomery, provider of melt pool width measurements; and Jason Fox, for his comments on the physics of the process.

REFERENCES

[1] The Economist, 2012. A third industrial revolution, April 21st.

[2] Bourell, D., Beaman, J., Marcus, H., and Barlow, J., 1990. "Solid freeform fabrication: An advanced manufacturing approach". In Proceedings of the International Solid Freeform Fabrication Symposium, pp. 1–7.

[3] Hull, C. W., 1986. Apparatus for production of three-dimensional objects by stereolithography, US Patent.

[4] Beaman, J., and Deckard, C., 1989. Selective laser sintering with assisted powder handling, US Patent.

[5] Foust, M. J., Thomsen, D., Stickles, R., Cooper, C., and Dodds, W., 2012. "Development of the GE aviation low emissions TAPS combustor for next generation aircraft engines". In 50th AIAA Aerospace Sciences Meeting including the new Horizons Forum and Aerospace Exposition, Vol. 936.

[6] Holshouser, C., Newell, C., Palas, S., Duty, C., Love, L., Kunc, V., Lind, R., Lloyd, P., Rowe, J., Dehoff, R., Peter, W., and Blue, C., 2013. "Out of bounds additive manufacturing". *Advanced Materials & Processes,* ***171***(3), pp. 15–17.

[7] Sundseth, J., and Berg-Johnsen, J., 2013. "Prefabricated patient-matched cranial implants for reconstruction of large skull defects". *Journal of central nervous system disease,* ***5***, pp. 19–24.

[8] Bauereiß, A., Scharowsky, T., and Körner, C., 2014. "Defect generation and propagation mechanism during additive manufacturing by selective beam melting". *Journal of Materials Processing Technology,* ***214***(11), pp. 2522–2528.

[9] King, W. E., Barth, H. D., Castillo, V. M., Gallegos, G. F., Gibbs, J. W., Hahn, D. E., Kamath, C., and Rubenchik, A. M., 2014. "Observation of keyhole-mode laser melting in laser powder-bed fusion additive manufacturing". *Journal of Materials Processing Technology,* ***214***(12), pp. 2915–2925.

[10] Gockel, J., Beuth, J., and Taminger, K., 2014. "Integrated

control of solidification microstructure and melt pool dimensions in electron beam wire feed additive manufacturing of Ti-6Al-4V". *Additive Manufacturing,* ***1***, pp. 119–126.

[11] Wu, A., Brown, D., Kumar, M., Gallegos, G., and King, W., 2014. "An experimental investigation into additive manufacturing-induced residual stresses in 316L stainless steel". *Metallurgical and Materials Transactions A,* ***45A***(13), pp. 6260–6270.

[12] Roberts, I. A., Wang, C. J., Esterlein, R., Stanford, M., and Mynors, D. J., 2009. "A three-dimensional finite element analysis of the temperature field during laser melting of metal powders in additive layer manufacturing". *International Journal of Machine Tools and Manufacture,* ***49***(12-13), pp. 916–923.

[13] Matsumoto, M., Shiomi, M., Osakada, K., and Abe, F., 2002. "Finite element analysis of single layer forming on metallic powder bed in rapid prototyping by selective laser processing". *International Journal of Machine Tools and Manufacture,* ***42***(1), pp. 61–67.

[14] Zeng, K., Pal, D., and Stucker, B. E., 2012. "A Review of Thermal Analysis Methods in Laser Sintering and Selective Laser Melting". In Proceedings of the Solid Freeform Fabrication Symposium, pp. 796–814.

[15] Jiang, W., and Dalgarno, K., 2002. "Finite Element Analysis of Residual Stresses and Deformations in Direct Metal SLS Process". In Solid Freeform Fabrication, pp. 340–348.

[16] Hussein, A., Hao, L., Yan, C., and Everson, R., 2013. "Finite element simulation of the temperature and stress fields in single layers built without-support in selective laser melting". *Materials & Design,* ***52***, pp. 638–647.

[17] Hodge, N., Ferencz, R., and Solberg, J., 2014. "Implementation of a thermomechanical model for the simulation of selective laser melting". *Computational Mechanics,* ***54***(1), pp. 33–51.

[18] Körner, C., Bauereiß, A., and Attar, E., 2013. "Fundamental consolidation mechanisms during selective beam melting of powders". *Modelling and Simulation in Materials Science and Engineering,* ***21***(8), p. 085011.

[19] Cheng, B., Price, S., Lydon, J., Cooper, K., and Chou, K., 2014. "On process temperature in powder-bed electron beam additive manufacturing: Model development and validation". *Journal of Manufacturing Science and Engineering,* ***136***(6), p. 061018.

[20] Moser, D., Beaman, J., Fish, S., and Murthy, J., 2014. "Multi-layer computational modeling of selective laser sintering processes". In International Mechanical Engineering Congress and Exposition.

[21] Ma, L., Fong, J., Lane, B., Moylan, S., Filliben, J., Heckert, A., and Levine, L., 2015. "Using design of experiments in finite element modeling to identify critical variables for laser powder bed fusion". In Proceedings of the International Solid Freeform Fabrication Symposium, pp. 219–228.

[22] King, W. E., Anderson, A. T., Ferencz, R. M., Hodge, N. E., Kamath, C., Khairallah, S. A., and Rubenchik, A. M., 2015. "Laser powder bed fusion additive manufacturing of metals; physics, computational, and materials challenges". *Applied Physics Reviews,* ***2***(4).

[23] Oden, T., Moser, R., and Ghattas, O., 2010. "Computer predictions with quantified uncertainty, Part I". *SIAM News,* ***43***(9), November, pp. 1–3.

[24] Roache, P., 2002. "Code verification by the method of manufactured solutions". *ASME Journal of Fluids Engineering,* ***114***(1), pp. 4–10.

[25] Kruth, J.-P., Mercelis, P., Van Vaerenbergh, J., and Craeghs, T., 2007. "Feedback control of selective laser melting". In Proceedings of the 3rd International Conference on Advanced Research in Virtual and Rapid Prototyping, Leiria, Portugal, Sept, Citeseer, pp. 24–29.

[26] Mani, M., Lane, B., Donmez, A., Feng, S., Moylan, S., and Fesperman, R., 2015. Measurement science needs for real-time control of additive manufacturing powder bed fusion processes. NISTIR 8036, National Institute of Standards and Technology.

[27] ASME V&V 20-2009, 2009. "Standard for verification and validation in computational fluid dynamics and heat transfer". *American Society of Mechanical Engineers*.

[28] Devesse, W., De Baere, D., and Guillaume, P., 2014. "The isotherm migration method in spherical coordinates with a moving heat source". *International Journal of Heat and Mass Transfer,* ***75***, pp. 726–735.

[29] Rosenthal, D., 1946. "The theory of moving sources of heat and its application to metal treatments". *Transactions of the ASME,* ***68***, pp. 849–866.

[30] Montgomery, C., Beuth, J., Sheridan, L., and Klingbeil, N., 2015. "Process mapping of inconel 625 in laser powder bed additive manufacturing". In Proceedings of the Solid Freeform Fabrication Symposium, pp. 1195–1204.

[31] Thermo-Calc, 2014. Thermo-Calc software AB version 3.1. Tech. rep.

[32] Kalman, R. E., 1960. "A new approach to linear filtering and prediction problems". *Journal of Basic Engineering - Transactions of the ASME,* ***82***(1), pp. 35–45.

[33] Vlasea, M., Lane, B., Lopez, F., Mekhontsev, S., and Donmez, A., 2015. "Development of powder bed fusion additive manufacturing test bed for enhanced real-time process control". In Proceedings of the International Solid Freeform Fabrication Symposium, pp. 527–539.

[34] Xiu, D., and Karniadakis, G. E., 2003. "Modeling uncertainty in flow simulations via generalized polynomial chaos". *Journal of computational physics,* ***187***(1), pp. 137–167.